sciendo

POLISH MARITIME RESEARCH 2 (114) 2022 Vol. 29; pp. 55-63
10.2478/pomr-2022-0017

EFFECTS OF RUDDER AND BLADE PITCH ON HYDRODYNAMIC PERFORMANCE OF MARINE PROPELLER USING CFD

Pham Ky Quang
School of Excellent Education, Vietnam Maritime University, Vietnam
Phan Van Hung
Faculty of Navigation, Vietnam Maritime University, Vietnam
Nguyen Chi Cong
Department of Mechanical Engineering, Vietnam Maritime University, Vietnam
Trinh Xuan Tung
School of Excellent Education, Vietnam Maritime University, Vietnam

* Corresponding author: *phanvanhung@vimaru.edu.vn (P. Van Hung)*

ABSTRACT

The use of computational fluid dynamics (CFD) to predict internal and external flows has risen dramatically in the past decade. This research aims to use the commercial software, ANSYS Fluent V.14.5, to illustrate the effects of the rudder and blade pitch on the hydrodynamic performance of the marine propeller by experimenting with propellers and rudders of the M/V Tan Cang Foundation ship, which has designed conditions as follows: diameter of 3.65 m; speed of 200 rpm; average pitch of 2.459 m; boss ratio of 0.1730. Using CFD, the characteristic curves of the marine propeller and some important results showed that the maximum efficiency of the propeller is 0.66 with the open water propeller and 0.689 with the rudder–propeller system at the advance ratio of 0.6. The obtained outcomes of this research are a significant foundation to calculate and design an innovative kind of propulsion for ships with high performance.

Keywords: Rudder; blade pitch; propeller; CFD

INTRODUCTION

At present, Computational Fluid Dynamics (CFD) plays an important role in simulating and calculating flow fields around different geometries using established algorithms. In recent years, considerable advances in the area of computer science have led to the decrease of the computational costs of CFD simulations, making them more accessible for practical applications, especially in the process of designing and optimising the ship and propeller.

Simulating the aforementioned experiments provides the opportunity to obtain desired results by analysing the calculated flow characteristics. This can be a practical way of obtaining valid results at relatively low costs and in a reasonable time compared with real experiments [1]. Since self-propulsion test simulation is still quite expensive and time-consuming, the common practice is to simulate only the open water test and to use its results to determine the self-propulsion characteristics. This can be done without taking into account factors including the interaction between the ship hull and the propeller. In 2003, Takayuki [1] used ANSYS Fluent software to study unsteady cavitation on a marine propeller. In his research, the Reynolds Averaged Navier–Stokes (RANS) model was solved to calculate and analyse the flow around a propeller with cavitation and non-cavitation. He found from his research that the CFD simulation results were in good agreement with the experiment [1]. Five years after his research, Bosschers also used the RANS method

and a boundary element method in which the acoustic wave equation is solved to examine the sheet cavitation of the propeller and the propeller–ship interaction. The achievements of the research were that the computational procedure can give reasonable and good results for the nominal wake field, the cavitation area, and the pressure fluctuation on the ship hull. The prediction of fluctuation on the ship hull for the model scale was more accurate than for the full-scale model [2]. Various numerical methods have been proposed based on the potential flow theory for the analysis of propellers. For instance, the combination of a panel method, which is also known as the Boundary Element Method (BEM), with a vortex lattice method was utilised to model the propeller [3]. Following Kinnas' project, in 2015, Chen used the RANS method to study the effect of scale on the hydrodynamic performance of a propeller and the results obtained are relatively appropriate to the experimental outcomes [4]. The RANS method combined with the k-ε turbulent viscous model was used to study the unsteady cavitating turbulent flow around a full-scale marine propeller [5]. In 2017, at the 10th International Conference on Marine Technology - MARTEC 2016, Banik got some results relating to the computation of the hydrodynamic characteristics of marine propellers using the induction factor method based on the normal induced velocity [6]. The significant results were that the normal induced velocity of a propeller can be obtained simply and accurately using the induction factor. The vortical theory based on Biot–Savart law [7] is used to find the induction factor, then the hydrodynamic characteristics of the propeller are estimated [6]. In addition to this area, the important results of simulating, analysing, and optimising the characteristics of a marine propeller were presented [8-10].

The results obtained from studying the effects of the geometry configuration on the hydrodynamic performance of a propeller suggested an innovative way to design a propeller including the effects of the wake flow and skew angle on the propeller's features [11-14]. Other authors found the effects of the rudder shape on the propeller's hydrodynamic characteristics in the propeller–rudder system, from which they suggested a useful way to improve the hydrodynamic performance of the propeller [15-16].

In addition, the propeller's hydrodynamic performance is also influenced by the shape and type of the rudder as well as the blade pitch. However, the number of studies on the performance of propellers due to the impact of these two factors is not great. Studying the impact of these two factors will be an important foundation to calculate and design a controllable pitch propeller whose blade pitch can change in operation, increasing the stability of the ship's manoeuvring.

MATHEMATICAL FOUNDATION

PARAMETERS OF PROPELLER'S HYDRODYNAMICS

According to the theory of the wing, the blade is divided into a large number of elementary strips, as seen in Fig. 1. Considering a blade element of the propeller's blade as shown in the figure, each of these elementary strips can then be regarded as an airfoil subject to a resultant incident velocity W. The resultant incident velocity is considered to comprise an axial velocity V together with a rotational velocity, which varies linearly up the blade.

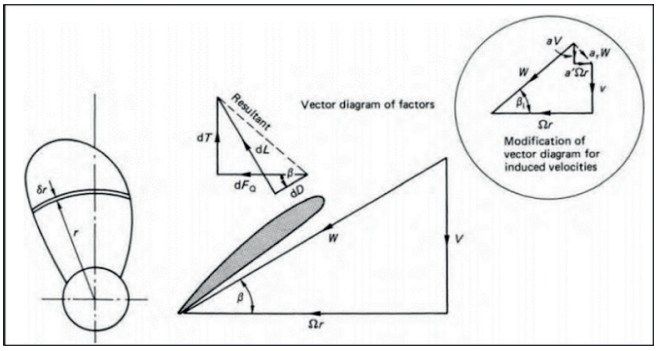

Fig.1. Blade element of the propeller's blade

The section will therefore experience lift and drag forces from the combination of this incidence angle and the section zero-lift angle, from which one can deduce that, for a given section geometry, the elemental thrust and torques are given by:

$$dT = \frac{1}{2}\rho.Z.c.W^2(c_l.\cos\beta - c_d.\sin\beta)dr$$
$$dQ = \frac{1}{2}\rho Zc.W^2(c_l.\sin\beta + c_d.\cos\beta)rdr \quad (1)$$

Therefore, the thrust and torque of a propeller can be found by integrating the formula:

$$T = \int_{r_h}^{r_t}\frac{1}{2}\rho.Z.c.W^2(c_l.\cos\beta - c_d.\sin\beta)dr$$
$$Q = \int_{r_h}^{r_t}\frac{1}{2}\rho.Z.c.W^2(c_l.\sin\beta + c_d.\cos\beta)rdr \quad (2)$$

where:
Z and c are the number of blades and the chord length of the section respectively.
c_l, c_d are the lift and drag coefficients of the profile at the specified radius.

From Formula (2), we find the characteristic coefficients of a propeller such as the thrust, torque, and efficiency coefficient. These coefficients can be defined as follows [7], [17-18]:

$$K_T = \frac{T}{\rho n^2 D^4}; K_Q = \frac{Q}{\rho n^2 D^5}; J = \frac{V_a}{nD}; \eta_0 = \frac{K_T.J}{K_Q.2\pi} \quad (3)$$

THE HYDRODYNAMIC FORCE ACTING ON THE RUDDER

The horizontal sectional shape of the rudder is symmetric and, just the same as the wing sections of an airplane, the rudder generates force by the steered angle shown in Fig. 2. The force is usually defined as the normal force N acting on the rudder's symmetrical plane and is shown as follows:

$$N = \frac{1}{2} c_N . \rho V_\infty^2 . A \quad (4)$$

Here:
α is the incident angle of inflow to the rudder that is made up of the rudder steered angle and the resultant flow of propeller slipstream and ship turning motion.
c_N is the normal force coefficient of the rudder section as a wing, being the function of the incident angle of inflow α.
A is the acting area of the rudder.
V_∞ is the inflow velocity coming up the rudder.

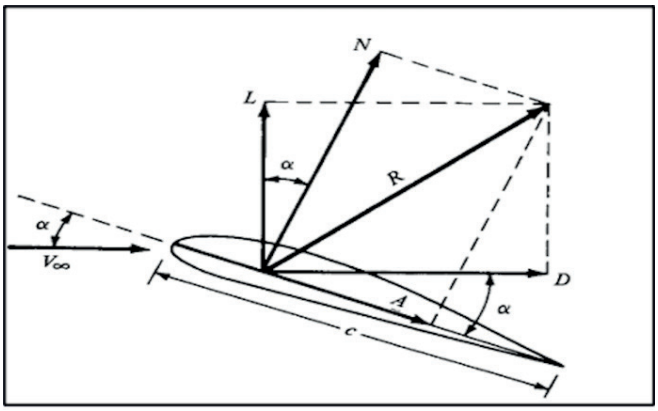

Fig. 2. The hydrodynamic force acting on a rudder

THEORETICAL CFD BASIS

A large number of problems related to fluid flows can be described by solving transport equations [19]. Transport equations are modelled in different ways, depending on the phenomenon that is considered, and so their form may differ. However, the behaviour of the dependent variables in all such equations is described with the same set of operators, which allows the formulation of the generic scalar transport equation. In the moving reference frame, the law of conservation of mass that was expressed by Euler is as follows [20]:

Conservation of mass

$$\frac{\partial \rho}{\partial t} + \nabla . \rho \vec{v}_r = 0 \quad (5)$$

Conservation of momentum

Newton's second law states that the rate of change in mass momentum of the fluid is equal to the net external force acting on the mass. Therefore, the equation of momentum conservation in the rotating frame is written as follows:

$$\frac{\partial}{\partial t}(\rho \vec{v}_r) + \nabla .(\rho \vec{v}_r . \vec{v}_r) + \rho(2\vec{\omega} \times \vec{v}_r + \vec{\omega} \times \vec{\omega} \times \vec{r} + \vec{a} \times \vec{r} + \vec{a}) = -\nabla p + \nabla \bar{\bar{\tau}} + \vec{F} \quad (6)$$

where $\vec{a} = \frac{d\vec{\omega}}{dt}$ and $\vec{a} = \frac{d\vec{v}_t}{dt}$

The stress tensor $\bar{\bar{\tau}}$ is given by

$$\bar{\bar{\tau}} = \mu \left[\left(\nabla \vec{v} + \nabla \vec{v}^T \right) - \frac{2}{3} \nabla \vec{v} I \right] \quad (7)$$

Turbulence model k–ε

Although turbulent flow is fully described by Navier–Stokes equations, it is characterised by a wide range of time and length scales, while the interactions between vortices are extremely non-linear. Such properties make turbulence hard to describe statistically, which certainly contributes to the complexity of predicting turbulent flow. To close the Navier–Stokes equation, in this research the authors use the turbulent model k-ε. The equation form of the k-ε turbulence is written as follows [20]:

$$\frac{\partial}{\partial t}(\rho k) + \frac{\partial}{\partial x_i}(\rho k u_i) = \frac{\partial}{\partial x_i}\left(\alpha_k \mu_{ef} \frac{\partial k}{\partial x_i} \right) + G_k + G_b - \rho\varepsilon - Y_M + S_k \quad (8)$$

and

$$\frac{\partial}{\partial t}(\rho \varepsilon) + \frac{\partial}{\partial x_i}(\rho \varepsilon u_i) = \frac{\partial}{\partial x_i}\left(\alpha_\varepsilon \mu_{ef} \frac{\partial \varepsilon}{\partial x_i} \right) + C_{1\varepsilon} \frac{\varepsilon}{k}(G_k + C_{3\varepsilon}.G_b) - C_{2\varepsilon} \rho \frac{\varepsilon^2}{k} - R_\varepsilon + S_\varepsilon \quad (9)$$

where: G_k represents the generation of turbulence kinetic energy due to the mean velocity gradients, G_b is the generation of turbulence kinetic energy due to buoyancy, Y_M represents the contribution of the fluctuating dilatation incompressible turbulence to the overall dissipation rate. The quantities α_k α_ε are the inverse effective Prandtl numbers for k and ε, respectively. S_k and S_ε are user-defined source terms. They are defined as follows:

$$G_k = -\rho\overline{u_i.u_j}\frac{\partial u_j}{\partial x_i}$$
$$G_b = \beta g_i \frac{\mu_t}{\Pr_t}\frac{\partial T}{\partial x_i}$$
$$S = \sqrt{2S_{ij}S_{ij}} \quad (10)$$
$$\beta = -\frac{1}{\rho}\left(\frac{\partial p}{\partial T}\right)_p$$

The other constants of the model are evaluated:

$$C_{1\varepsilon} = 1,44, C_{2\varepsilon} = 1,92, C_\mu = 0,09, \sigma_k = 1, \sigma_\varepsilon = 1,3$$

CALCULATION AND SIMULATION

THE STUDIED CASES

This research aims to illustrate the effects of the rudder and blade pitch on the hydrodynamic performance of the marine propeller, and the authors analysed the specific cases as follows:

The first case: To cope with the effects of the blade pitch on the propeller's hydrodynamic features, the team calculated and simulated the open water with advanced ratio J changing from 0.1 to 0.75 and the attack angle of the blade in the range of -7 to +7 degrees.

The second case: To study the effects of the rudder on the hydrodynamic characteristics of the propeller, the authors calculated and simulated open water and the propeller in the rudder-propeller system with an advanced ratio changed J from 0.1 to 0.75.

MODEL, FLUID DOMAIN, AND MESH

The propeller and rudder studied in this article are those fitted in the M/V Tan Cang Foundation. The crucial parameters of the propeller and rudder are given in Tables 1 and 2 below. The rudder is installed on the aft side of the propeller and the position between the rudder and propeller is displayed in Fig. 3.

Tab. 1. Propeller detail parameters

No	Parameter	Value	Unit
1	Diameter	3.650	m
2	Pitch	2.459	m
3	Design rate of revolutions	200	rpm
4	Number of blades	4	
5	Rake	10	deg
6	Skew	25	deg
7	Blade thickness ratio	0.049	10
8	Blade section	NaCa 66, a = 0.8	

Tab. 2. Rudder detail parameters

No	Parameter	Value	Unit
1	Rudder height	4,8	m
2	Chord length of the top section	3,45	m
3	Chord length of the bottom section	2.45	m
4	Rudder area	12	m^2
5	Rudder profile	NaCa 0018	

The three characteristic curves of a propeller consist of the thrust, torque, and efficient curves corresponding to the different advanced velocities of its ship. To construct these curves of the investigated propeller by the numerical method, the first step in the process is to build a suitable fluid domain covering the propeller. In this work, the domain is a cylinder, as shown in Fig. 3, with a length of 13 times the propeller's diameter and a diameter of seven times the propeller's diameter, divided into two components: the static domain and the rotating domain. In the third step, the domain is imported, meshed, and refined in the ANSYS meshing ICEM tool. All domains are meshed by using tetra mesh, in which the rotating domain is modelled with smooth mesh, and the static domain takes coarse mesh, which is then converted into polyhedral mesh to save calculation time and improve the accuracy of the simulation results.

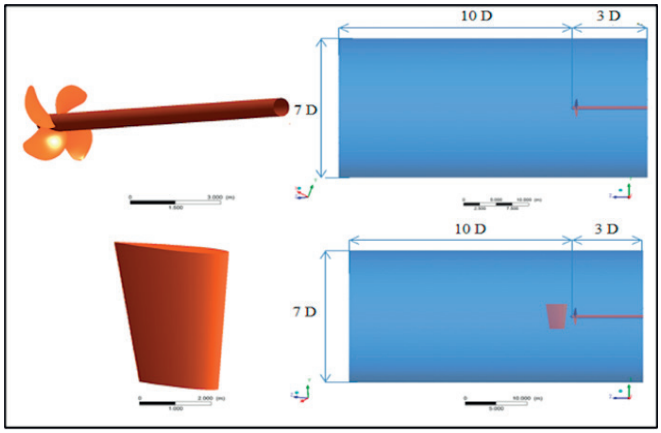

Fig. 3. The propeller, rudder, and computed fluid domain

MESH VALIDATION

The quality of the computational grid plays an important role and directly affects the convergence and results of numerical analysis. To determine the mesh's independence of the calculation results, the team employed calculations for nine different mesh numbers to specify the most suitable number. These calculations are carried out at the advance ratio J of 0.2, and the dependence of the mesh number on the calculation results in the two cases, the open water, and the rudder-propeller system, is shown in Fig. 1. To ensure accuracy, the mesh number for all calculations has to be larger than 325000 polyhedral elements, as shown in Fig. 1. Therefore, the team finally selected the five cases in which the

mesh element number in the two cases is 631646 and 682736 elements respectively for all calculations. The investigated geometry domain and mesh are presented in Fig. 4 and Fig. 5.

Tab. 3. Detailed mesh for computation

	Open water (free propeller)		Propeller–rudder system	
Domain	**Elements**	**Polyhedra**	**Elements**	**Polyhedra**
Dynamic fluid	326437	326437	326437	326437
Static fluid	305209	305209	356299	356299
All domains	631646	631646	682736	682736

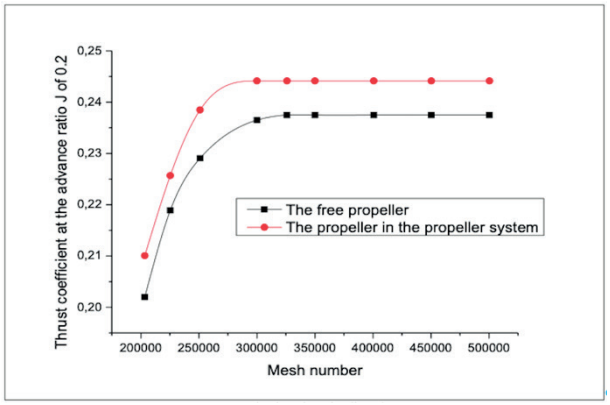

Fig. 4. Mesh independence for all domains

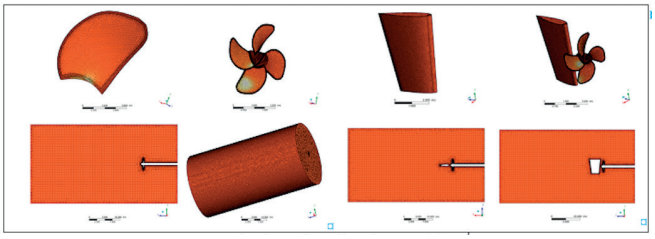

Fig. 5. Mesh on the propeller, rudder, and investigated domain

BOUNDARY CONDITION

To solve the problem in this article, the turbulent RNG kε model is chosen as the turbulence model to close the Reynolds averaged equations. The velocity inlet, which is axially uniform, has a magnitude equalling the ship's advance velocity and is selected as an inlet boundary condition [20-22]. The pressure outlet is specified as the outlet boundary condition, and the gauge pressure on the outlet is set to 0 Pa. With wall boundary conditions, the no-slip condition is enforced on the wall surface and the standard wall function is also applied to an adjacent region of the walls. A moving reference frame (MRF) is used to establish the moving coordinate system rotating with the propeller synchronously and the stationary coordinate system fixed on the static shaft of the propeller, respectively. The first-order upwind scheme with numerical underrelaxation is applied for the discretisation of the convection term and the central difference scheme is employed for the diffusion term. The pressure–velocity coupling is solved through the PISO algorithm. The convergence precision of all residuals is under 0.0001.

RESULTS AND ANALYSIS

CHARACTERISTICS OF OPEN WATER PROPELLER

Fig. 6 shows the pressure distribution on the back and pressure face of the studied propeller at the advance ratios J of 0.1 and 0.6. The principle of distribution pressure on the two faces of the blade satisfies the theoretical law of the axial turbomachinery. There is a pressure difference between the pressure face and the back face of the propeller in operation, and that difference makes the propeller thrust to overcome the ship hull resistance. The pressure distribution on the two faces of the blade mainly depends on the advance ratio J or velocity inlet; the smaller the advance ratio, the higher the thrust. At the operating condition of the ship J = 0.6, on the pressure face, most of the area of the blade has the pressure value of about 2–4×10⁴ Pa, while most of the area of the suction face has a pressure around 4×10⁴ Pa. This means that the fluid accelerates as it approaches the propeller due to low pressure in the front of the propeller and the water continues to accelerate when it leaves the propeller.

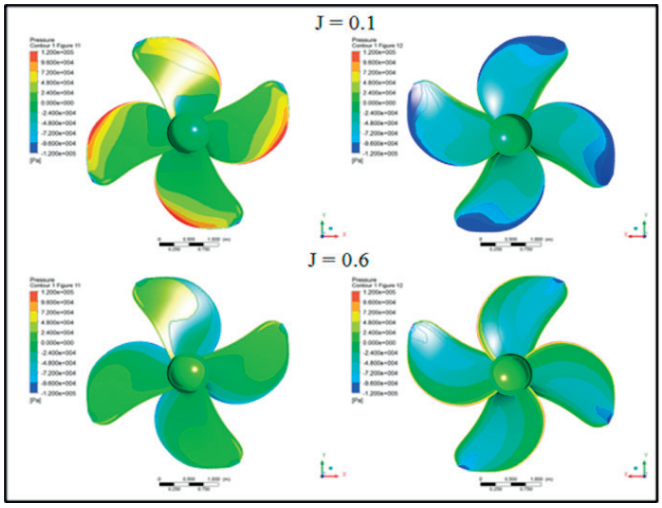

Fig. 6. Pressure distribution on the faces of the propeller at J of 0.1 and 0.6

Fig. 7 illustrates the hydrodynamic performance curves of the propeller corresponding to the different advanced ratios J. As can be seen from Fig. 7, it was tracked by numerical simulations, the changing principle of the thrust and torque coefficient decreases gradually when the advance ratio J rises, and the maximum thrust and torque coefficients are 0.283, 0.032 respectively at the advance ratio J of 0.1. The efficiency curve is slightly different in that it conforms to the linear principle with a small advance ratio in the range of 0.1–0.4, and the maximum efficiency is 0.66 with an advance ratio J of 0.6 at the initially designed optimal point.

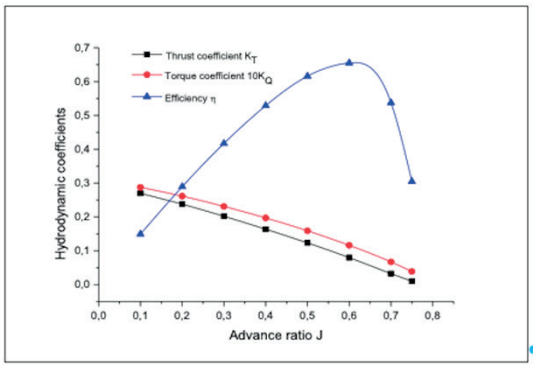

Fig. 7. The propeller characteristic curves

EFFECTS OF THE RUDDER ON HYDRODYNAMIC PERFORMANCE OF THE PROPELLER

In this section, the effects of the rudder in the rudder–propeller system on the hydrodynamic performance of the propeller are investigated by using the numerical method. The two models of the propeller with and without a rudder are computed in the same condition to compare the hydrodynamic performance. Fig. 8 shows the CFD results of the pressure distribution on the propeller's faces at an advance ratio J of 0.6.

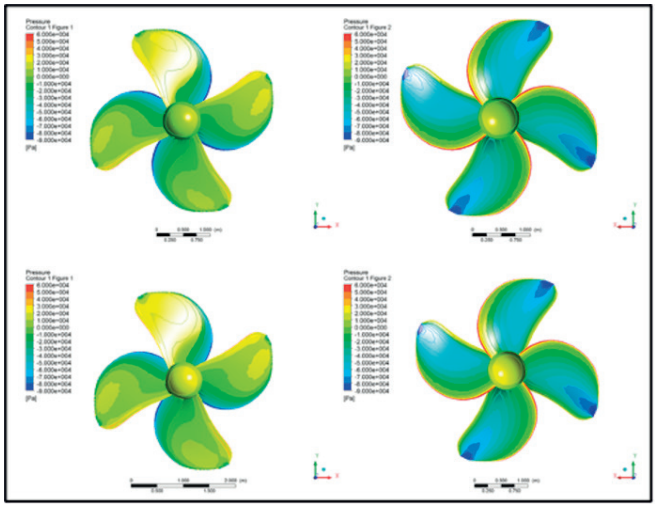

Fig. 8. Pressure distribution on two faces of the propeller in both cases at J = 0.6

Fig. 8 reveals the pressure distribution on the back face and pressure face of the propeller in both cases at the advance ratio J of 0.6. As can be seen, the pressure distribution on the back face of the propeller in both cases is relatively similar, while the distribution pressure of the pressure face of the propeller in the propeller–rudder system and the open-water propeller is slightly different, especially in the region of the propeller hub. In the propeller–rudder system, the propeller thrust goes up compared with the open-water propeller because the low-pressure area on the hub decreases, and the pressure face's high-pressure area near the blade tip increases. The pressure value in this region is about 1–2×10^{-4} Pa. The propeller's thrust in this case also increases; however, the rise of the propeller thrust is higher than the increase of the torque acting on the propeller. As a result, the propeller efficiency in the propeller–rudder system increases slightly.

Fig. 9 reveals the characteristic curves of the propeller in the two cases. From Fig. 9, we can recognise that the efficiency of the propeller in the propeller–rudder system is slightly higher than the efficiency in the open water. The higher the advance ratio of the vessel, the greater the efficiency of the propeller. At the designed optimal point of the propeller corresponding to the exploited velocity of the vessel, the propeller's efficiency in the propeller–rudder system increases by about 4.8 %.

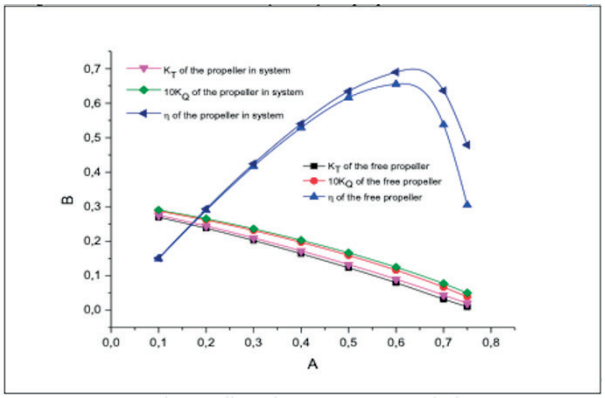

Fig. 9. The propeller's characteristic curves in both cases

EFFECT OF THE PROPELLER ON THE RUDDER'S HYDRODYNAMIC FEATURES

Fig. 10 presents the vector velocity going out of the propeller, and the pressure distribution of the rudder's faces. It can be seen from this figure that the velocity field on the aft side of the propeller is not uniform, and the flow's vector inclines with the rudder's symmetry plane at any angle. This makes the pressure distribution of the rudder faces asymmetric and the maximum pressure reaches about 6×10^4 Pa in the region corresponding to the propeller's blade tips. As a result, it is not only the drag on the rudder but also the vertical force appearing on the rudder. The rudder's drag changes in a nearly linear function of advance ratio J, and the maximum drag of the rudder is 16 kN at the advance ratio J of 0.75. On the other hand, the vertical force is a curve of advance ratio J, and reaches a maximum value of about 4 kN, corresponding to J of 0.5. At a small velocity, it increases dramatically, while at the advance ratio J in the range of 0.5–0.75, it decreases slightly. The changing principle of the forces is given in Fig. 10.

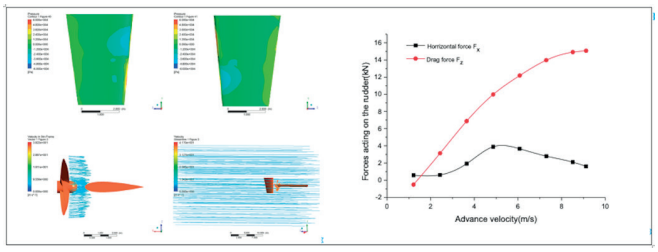

Fig. 10. Pressure distribution on the rudder and flow's velocity vector on the aft side of the propeller and the forces on the rudder

EFFECTS OF BLADE PITCH ON THE PROPELLER'S HYDRODYNAMIC PERFORMANCE

In this section, the numerical method is used to investigate the effects of the blade pitch on the hydrodynamic performance of the propeller. From the results of the comparison of various models with different blade pitch angles, the effects of the blade pitch angle on the hydrodynamic performance of the propeller are shown. In this research, the blade pitch angle of the propeller is changed from -7 to +7 degrees. The computational condition is the same for all models. Fig. 11 shows the results of the pressure distribution on faces with different blade pitches at the advance ratio J of 0.4.

As can be seen from Fig. 11, the blade pitch has a significant impact on the distribution pressure of the propeller blade's surfaces. At the pitch of -7 degrees, on the pressure face, the maximum pressure is 7.2×10^4 Pa at the trailing edge, and the minimum value is 1.2×10^5 Pa at the leading edge. At the back face, the maximum value reaches 1.2×10^5 Pa at the leading edge, and the minimum value is 1.2×10^5 Pa at the blade's tip. On the contrary, at the pitch of 7 degrees, there is a dramatic change in the pressure distribution of the blade's faces. The maximum pressure value on the back face is 1.2×10^5 Pa at the leading edge, and the minimum value is 1.2×10^5 Pa on the small area at the blade's tip. On the back face, these are 4×10^4 Pa and 1.2×10^5 Pa at the trailing edge and leading edge. As a consequence, the propeller thrust increases steadily when the blade pitch rises.

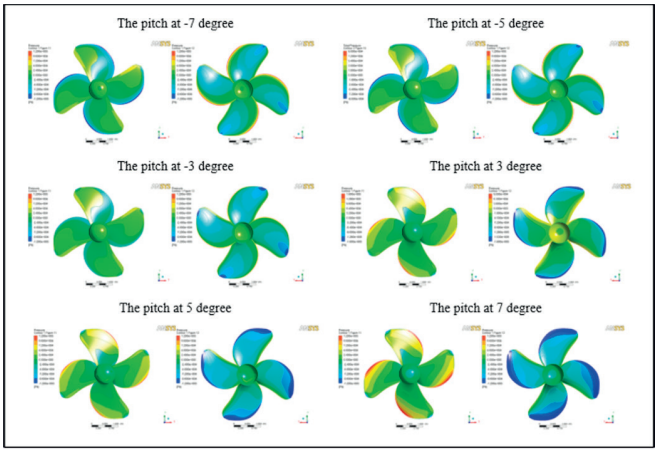

Fig. 11. Pressure distribution on propeller's faces with different blade pitches of -7, -5, 5, and 7 degrees at J = 0.4

Fig. 12 presents the thrust and torque coefficients of the investigated propeller at different blade pitches. It can be seen from this figure. that the thrust and torque coefficient decreases gradually when the blade pitch goes down. The maximum thrust and torque coefficients are 0.41 and 0.06 respectively, corresponding to the blade pitch of 7 degrees. The minimum thrust and torque coefficients are 0.0075 and 0.0038, corresponding to the blade pitch of -7 degrees.

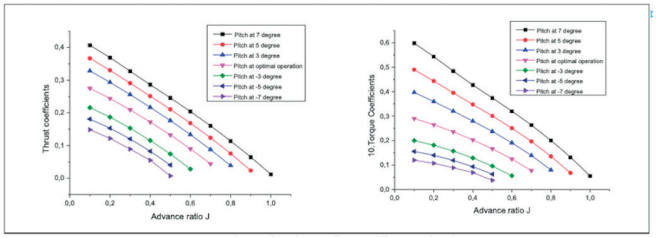

Fig. 12. The propeller's thrust coefficient at different attack angles

Fig. 13 shows the propeller's efficiency at different pitches. We can see from this figure that the propeller's efficiency changes to the principle of the axial turbomachinery and it is a function of the advance ratio J at each pitch. In the investigated pitches, the propeller's efficiency rises dramatically when the blade pitch increases. The maximum efficiency of the propeller is 0.72, corresponding to the advance ratio J of 0.8 at the blade pitch of 7 degrees. However, at the specific pitch, the propeller's efficiency always has the extremum corresponding to the specific advance ratio J. This is significant with controllable pitch propellers, in which their blade pitch can change to adjust to the load acting on a vessel in operation. With a propeller of this type, the general characteristic curve is a set of characteristic curves at different pitch ratios, so in each specific operating condition of a ship, the propeller can change the blade pitch to achieve high efficiency without altering the revolutions of the engine shaft.

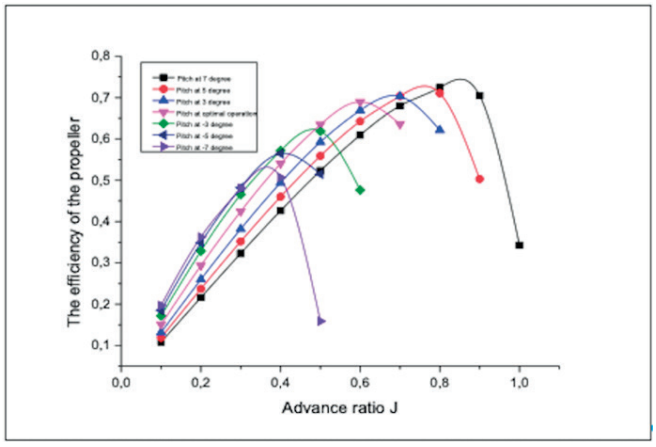

Fig. 13. The efficiency of the propeller at different attack angles

CONCLUSION

In this paper, the propeller, and rudder of the M/V Tan Cang Foundation ship are analysed at different advance ratios to construct the hydrodynamic performance curves. The effects of the rudder and blade pitch angle of the propeller are investigated and some of the obtained results are presented in the paper.

This paper covers the process of CFD used to construct the propeller's characteristic curves, from which the team investigates the effects of the blade pitch and rudder on the hydrodynamic features of the marine propeller.

The simulation results achieved, such as the pressure, velocity distribution, and characteristic curves, are appropriate to the turbomachinery theory and have reasonable accuracy.

The characteristic propeller curves are constructed by using the MRF and RNG k-ε model in ANSYS Fluent 14.5. The maximum efficiency of the propeller is 0.66 with the open water propeller and 0.689 with the rudder–propeller system at an advance ratio of 0.6.

The results obtained reveal that the rudder has a slight effect on the propeller's hydrodynamic characteristics. At the designed optimal point of the studied propeller, the efficiency in the rudder–propeller system rises by about 4 % compared with the open-water propeller. On the contrary, the propeller also has a significant impact on the hydrodynamic features of the rudder. The interaction between the propeller and the rudder creates a horizontal force on the rudder in the ship operation, this force reaching the maximum value of 4.5 kN corresponding to the advance ratio J = 0.4. The force-generating in this interaction reduces the stability of the ship's manoeuvring.

The blade pitch also has important effects on the hydrodynamic characteristics of the propeller. When the blade pitch rises, in the investigated pitch, the thrust, and torque coefficient of the propeller increase dramatically. This is an important foundation to calculate and design a controllable pitch propeller in which its blade pitch can change in operation. The general characteristic curves of this type of propeller are a set of curves at different pitches, so a ship equipped with a controllable pitch operating in the specific condition usually achieves high efficiency when compared with a fixed propeller having the same geometry characteristics

ACKNOWLEDGEMENT

The authors would like to thank all colleagues at Vietnam Maritime University for their assistance during the work. Additionally, we appreciate the constructive suggestions of the anonymous reviewers, which are invaluable in improving the quality of the manuscript.

REFERENCES

1. Y. Zhang, X. P. Wu, M. Y. Lai, G. P. Zhou, and J. Zhang, "Feasibility Study of Rans in Predicting Propeller Cavitation in Behind-Hull Conditions", Polish Marit. Res., vol. 27, no. 4, 2020, DOI: 10.2478/pomr-2020-0063.

2. M. Burak Samsul, "Blade Cup Method for Cavitation Reduction in Marine Propellers", Polish Marit. Res., vol. 28, no. 2, 2021, DOI: 10.2478/pomr-2021-0021.

3. S. A. Kinnas, Y. Tian, A. Sharma, "Numerical Modeling of a Marine Propeller Undergoing Surge and Heave Motion", International Journal of Rotating Machinery, pp. 1-8, 2012, doi.org/10.1155/2012/257461

4. A. Nadery and H. Ghassemi, "Numerical Investigation of the Hydrodynamic Performance of the Propeller behind the Ship with and without Wed", Polish Marit. Res., vol. 27, no. 4, 2020, DOI: 10.2478/pomr-2020-0065.

5. Y. Zhang, X. P. Wu, M. Y. Lai, G. P. Zhou, and J. Zhang, "Feasibility Study of RANS in Predicting Propeller Cavitation in Behind-Hull Conditions", Polish Marit. Res., vol. 27, no. 4, 2020, DOI: 10.2478/pomr-2020-0063.

6. H. Nouroozi and H. Zeraatgar, "Propeller Hydrodynamic Characteristics in Oblique Flow by Unsteady Ranse Solver", Polish Marit. Res., vol. 27, no. 1, 2020, DOI: 10.2478/pomr-2020-0001.

7. B. Lou and H. Cui, "Fluid-structure interaction vibration experiments and numerical verification of a real marine propeller", Polish Marit. Res., vol. 28, no. 3, 2021, DOI: 10.2478/pomr-2021-0034.

8. L. Guangnian, Q. Chen, and Y. Liu, "Experimental Study on Dynamic Structure of Propeller Tip Vortex", Polish Marit. Res., vol. 27, no. 2, 2020, DOI: 10.2478/pomr-2020-0022.

9. S. E. Belhenniche, M. Aounallah, O. Imine, F. Celik, "Effect of geometry configurations on hydrodynamic performance assessment of a marine propeller", Journal of Shipbuilding, vol. 67, no. 4, pp. 31-48, 2017. doi:10.21278/brod67403

10. G. Kuiper, "New developments and propeller design", Journal of Hydrodynamics, vol.7, no. 22, pp. 7-16, 2010. doi:10.1016/S1001-6058(09)60161-X

11. A. Farkas, N. Degiuli, I. Martić. "Assessment of the effect of biofilm on the ship hydrodynamic performance by performance prediction method", Int. J. Naval Architecture and Ocean Engineering, vol. 13, pp. 102-114, 2021. https://doi.org/10.1016/j.ijnaoe.2020.12.005.

12. S. Gaggero, "Design of PBCF energy saving devices using optimization strategies: A step towards a complete viscous design approach", Ocean Engineering, vol. 159, pp. 517-538, 2018. doi://doi.org/10.1016/j.oceaneng.2018.01.003.

13. V. H. Ngo, T. T. Le, Q. Le, Y. Ikeda, "A study on interaction effects on hydrodynamic performance of a system rudder-propeller by distant gap", Proceedings of the 12th International Marine Design Conference, Tokyo, Japan, pp. 179-193, 2015.

14. V. H. Ngo, T. T. Le, Y. Ikeda, "A study on improving hydrodynamic performances of a system rudder and propeller by attaching a fix plate on the rudder", The 8th Asia-Pacific Workshop on Marine Hydrodynamics - APHydro 2016, Hanoi, Vietnam, pp. 277-284, 2016.

15. P. B. John, A. Poul, Hydrodynamics of Ship Propellers Cambridge University Press, 2010. https://doi.org/10.1017/CBO9780511624254

16. H. Ira, A. Abbott, E. Von Doenhoff, Theory of Wing Sections, Dover Publications, New York, 1958. Available: https://catalog.library.vanderbilt.edu/permalink/01VAN_INST/13em2a7/alma991043239434003276

17. J. S. Carlton, Marine Propellers and Propulsion (Fourth Edition), Butterworth-Heinemann, 2019. https://doi.org/10.1016/C2014-0-01177-X

18. ANSYS Fluent Theory Guide, 2013.

19. ITTC, Proc. of the 25th International Towing Tank Conference, Fukuoka, Japan, 2008. Available: http://resolver.tudelft.nl/uuid:76a73833-cd0a-4972-9540-b56659b8cdab

20. ITTC, Proc. of the 26th International Towing Tank Conference, Rio de Janeiro, Brazil, 2011. Available: https://ittc.info/media/3317/committees.pdf

CONTACT WITH THE AUTHORS

Pham Ky Quang
e-mail: phamkyquang@vimaru.edu.vn

School of Excellent Education,
Vietnam Maritime University
No. 484 Lach Tray, Kenh Duong, Le Chan,
180000 Hai Phong
Vietnam

Phan Van Hung
e-mail: phanvanhung@vimaru.edu.vn

Faculty of Navigation,
Vietnam Maritime University
No. 484 Lach Tray, Kenh Duong, Le Chan,
180000 Hai Phong
Vietnam

Nguyen Chi Cong
e-mail: nguyenchicong@vimaru.edu.vn

Department of Mechanical Engineering,
Vietnam Maritime University
No. 484 Lach Tray, Kenh Duong, Le Chan,
180000 Hai Phong
Vietnam

Trinh Xuan Tung
e-mail: trinhxuantung@vimaru.edu.vn

School of Excellent Education,
Vietnam Maritime University
No. 484 Lach Tray, Kenh Duong, Le Chan,
180000 Hai Phong
Vietnam